Biosensors and Bioelectronics 145 (2019) 111732

Contents lists available at ScienceDirect

Biosensors and Bioelectronics

journal homepage: http://www.elsevier.com/locate/bios

An amplified label-free electrochemical aptasensor of γ-interferon based on target-induced DNA strand transform of hairpin-to-linear conformation enabling simultaneous capture of redox probe and target

Hui Jin [1], Rijun Gui [1,*], Xiaohui Gao, Yujiao Sun

College of Chemistry and Chemical Engineering, Intellectual Property Research Institute, Qingdao University, Shandong, 266071, PR China

ARTICLE INFO

Keywords:
Electrochemical aptasensor
Label-free biosensor
Interferon
MoS_2 nanosheet
Dendrimer

ABSTRACT

In this work, a novel and signal-amplified label-free electrochemical aptasensor was developed and enabled efficient determination of γ-interferon (IFN-γ), based on target-induced DNA strand transform of hairpin-to-linear conformation combining with simultaneous capture of redox probe and target. Gold nanoparticles (AuNPs) were electrodeposited in the matrix of poly(amidoamine) dendrimer (PAMAM), followed by drop-casting addition on MoS_2 nanosheets to prepare AuNPs- PAMAM/MoS_2 composites. HS-terminated hairpin-DNA aptamer of IFN-γ was conjugated with AuNPs to prepare aptamer-AuNPs-PAMAM/MoS_2 onto glassy carbon electrode (GCE), by using bovine serum albumin as the cross-linker and stabilizer. Methylene blue (MB) as a redox probe was absorbed on IFN-γ aptamer. In the presence of IFN-γ, MB electrochemical signal increased gradually. The preparation processes, mechanisms and optimal experiment conditions of aptamer- AuNPs-PAMAM/MoS_2/MB/GCE sensing platform were studied by electron microscope imaging technologies, spectral curves and electrochemical measurements. There is a well plotting linear relationship between the peak current intensities of MB and IFN-γ contents in the range of 0.01–1000 pg mL^{-1}, showing a low detection limit of 2 fg mL^{-1}. Experimental results testified that the aptasensor had highly sensitive and selective responses toward IFN-γ, over potential interferents. In real biological samples, the aptasensor of IFN-γ had superior detection recoveries, indicating its high detection performance and feasibility for practicability.

1. Introduction

As one category of cell-secreted factors, Interferon-Gamma (IFN-γ), also known as macrophage activating factor, is the only member of type-II Interferon (Schroder et al., 2004; Boehm et al., 1997). The disorder of IFN-γ secretion is associated with many diseases, such as inflammatory bowel disease, genital herpes simplex virus infection, Alzheimer's disease, and so forth (Dowlati et al., 2010; Biron et al., 1999; Omae et al., 2018; Jager et al., 2003; Akter et al., 2012; Cohen and Walt, 2018). Sensitive detection of IFN-γ is conducive to the activity study of immune responses and the diagnosis of infectious diseases. Enzyme-linked immunosorbent assay is frequently used to quantitatively and qualitatively determine IFN-γ, which can determine whether human body is infected with *Mycobacterium tuberculosis* (Golichenari et al., 2018). Cytokines are often detected by antibody immunoassays, but the methods require a long time, multiple washing and multi-step treatments to obtain the readout results (Akter et al., 2012; Cohen and Walt, 2018). Owing to the requirements of some complicated washing and labeling operations, a dynamic monitoring of cell secretions is hard to perform through depending on detection of antibodies. Besides, the efficiency of enzymatic catalytic reaction is variable, which may cause the fluctuation of output signals. This defect will restrain the reproducibility of detection results and lead to prolonged analysis time.

As emerging and effective artificial alternatives to antibodies, DNA nucleic acid aptamers have many merits, such as high thermal and chemical stability, reproducibility and easy of modification, which have attracted much attention of numerous scientists. Currently, scientists have developed a series of aptasensors based upon the specific binding of DNA nucleic acid aptamers with ligands (Wang et al., 2016). As for distinctive features of aptasensors, an oligonucleotide is designed and serves as the beacons that can produce signal directly upon the binding of oligonucleotides with targets, without labeling and washing

* Corresponding author.
E-mail address: guirijun@qdu.edu.cn (R. Gui).
[1] These authors have the equivalent contribution to this work.

https://doi.org/10.1016/j.bios.2019.111732
Received 17 July 2019; Received in revised form 23 September 2019; Accepted 25 September 2019
Available online 27 September 2019

procedures (Wen et al., 2018; Xia et al., 2015; Zhou et al., 2018). Detection process of aptasensors for ligand molecules is facile, endowing aptasensors great prospect for versatile applications. Aptasensors are especially suitable for real-time and dynamic detection of targets in biological samples.

Electrochemical aptasensors involve aptamers as molecular recognition elements. Aptamers are fixed to a signal converter, followed by connection through electronic wire to construct the sensor. Based on electrochemistry methods, electrochemical aptasensors enable qualitative or quantitative determination of various targets (Jin et al., 2018b). Compared with conventional electrochemistry analysis methods (Gao et al., 2018, 2019; Jin et al., 2017, 2018a; Guo et al., 2017a, 2017b), electrochemical aptasensors have significant advantages for biomolecule detection, such as high sensitivity, broad detection range, facile preparation, excellent selectivity, accuracy and reproducibility (Golichenari et al., 2018; Wang et al., 2016; Wen et al., 2018; Xia et al., 2015; Zhou et al., 2018; Jin et al., 2018b). Previously, scientists explored an immunoglobulin strategy for IFN-γ detection through the specific binding of oligonucleotide aptamers with ligand molecules (Liu et al., 2015b). Redox probes (methylene blue, ferrocene) were employed to label the aptamer of IFN-γ and the labelled probes were assembled onto an electrode through electrode interface modifications. The measured electrochemical signal intensities and changes can perform the quantification of IFN-γ contents. The aptamers-functionalized electrodes enabled the detection of cell-secreted factors (α-interferon, IFN-γ). Besides, Abnous et al. designed an electrochemical aptasensor of IFN-γ, based on the use of a three-helix molecular switch and methylene blue as a redox probe (Abnous et al., 2017).

Label-free electrochemical aptasensors have attracted much interest of researchers because they possess many unique merits, such as simple construction, free of aptamer-labelling and low cost, when compared with traditional aptamer-labelled electrochemical aptasensors (Jin et al., 2018b; Shamsipur et al., 2015; Ding et al., 2017; Yan et al., 2013). In this work, we proposed a novel and facile amplified label-free electrochemical aptasensor for sensitive detection of IFN-γ (Scheme 1). Herein, the target IFN-γ caused a transform of DNA strands from hairpin to linear conformations, which enabled simultaneous capture of redox probes and the target. The specific aptamer-ligand combination process was accompanied with the recognition of IFN-γ and the adsorption of redox probes, which hence generated an amplified signal on electrode interface. MoS_2 nanosheets were prepared by ultrasonication exfoliation. Gold nanoparticles (AuNPs) were electrodeposited in the matrix of poly(amidoamine) (PAMAM) dendrimers. After the drop-by-drop addition of AuNPs- PAMAM on MoS_2 nanosheets under stirring, AuNPs-PAMAM/MoS_2 composites were prepared and dropped-casting on Nafion-modified glassy carbon electrode (GCE) interface. HS-terminated hairpin-DNA aptamer of IFN-γ was conjugated with AuNPs through Au–S coupling to prepare the aptamer-AuNPs-PAMAM/MoS_2/GCE sensing platform, by using bovine serum albumin (BSA) as a cross-linker or stabilizer. Methylene blue (MB) as a redox probe was absorbed on IFN-γ aptamer through hydrogen bond, intermolecular force and non-covalent interactions, which exported weak electrochemical signal of MB. In the presence of IFN-γ, a hairpin conformation of single-strand DNA aptamer was transferred into a linear one. The transform came from specific combination of IFN-γ with its aptamer, which was stronger than base complementary pairing in hairpin aptamers. Linear aptamers have superior adsorption action over hairpin ones. The more MB was absorbed on linear aptamers and had an enhanced electrochemical

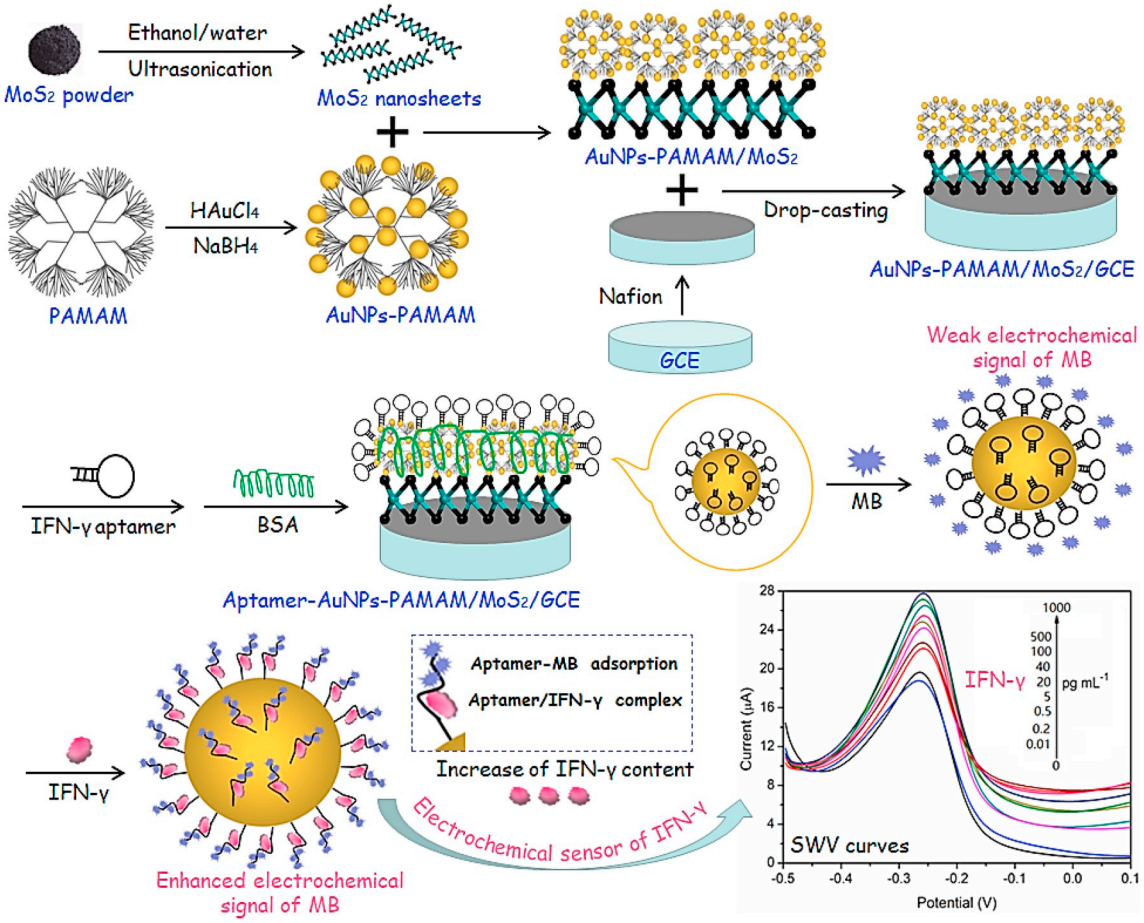

Scheme 1. Schematic illustration of preparation routes and applications of aptamer-AuNPs-PAMAM/MoS_2/GCE sensing platform as an amplified label-free electrochemical aptasensor of IFN-γ.

signal of MB. With the increase of IFN-γ contents, electrochemical signal of MB increased gradually. A novel, facile and signal-amplified label-free electrochemical aptasensor was explored for efficient detection of IFN-γ.

2. Experimental section

2.1. Chemicals

MoS_2 powder was purchased from Zhengzhou Cheng'ao Chemical Products Co., Ltd., China. PAMAM dendrimer G5-NH_2 came from Xi'an Ruiyu Biotechnology Co., Ltd., China. IFN-γ, MB, BSA, ascorbic acid (AA), cysteine (L-cys), uric acid (UA), glucose, myoglobin, immunoglobulin G (Ig G), interleukin-22 (IL-22), Nafion and other biological reagents were bought from Shanghai Sangon Biotech Co., Ltd., China. $HAuCl_4{\cdot}4H_2O$, $NaBH_4$, Tris-HCl, $K_3Fe(CN)_6$, ethanol and other chemicals with the analytical grate were purchased from Shanghai Sinopharm Chemical Reagent Co., Ltd., China. HS-terminated hairpin-DNA aptamer of IFN-γ with artificial base sequences of 5′-GGGG TTGG TTGT GTTG GG TGTT GTGT CCAA CCCC-C_6-SH-3′ was synthesized and purified by Shanghai Sangon Biotech Co., Ltd., China. All chemicals and biological reagents can be directly used as received without purification. Phosphate buffered saline (PBS) solution was prepared by mixing Na_2HPO_4 and NaH_2PO_4 and used for pH adjustments. Doubly distilled water (DDW) was used in experiments. Human serum samples selected from healthy young volunteers were provided by a local hospital.

2.2. Apparatus

Transmission electron microscope (TEM) images were recorded on a JEM-1200 TEM operated at an acceleration voltage of 120 kV (Jeol, Japan). UV–vis absorption spectra were measured with a UV-2800A spectrophotometer (Unico, China). Fourier transform infrared (FT-IR) spectroscopy measurements were performed with an iS50 FT-IR spectrometer with KBr window in transmission mode (Nicolet, USA). Cyclic voltammetry (CV), electrochemical impedance spectroscopy (EIS) and square wave voltammetry (SWV) curves were characterized with a CHI-660E electrochemical workstation (Chenhua, China). A conventional three-electrode system was used in measurements, including a GCE as working electrode, a saturated calomel electrode (SCE) as reference electrode and a platinum wire as counter electrode. Electrochemical measurements were conducted for three repeats. Each result was expressed as the average of repetitive measurements.

2.3. Preparation of MoS_2 nanosheets, AuNPs-PAMAM and AuNPs-PAMAM/MoS_2 composites

MoS_2 nanosheets were prepared through liquid-phase exfoliation (Zhou et al., 2014; Li and Du, 2017). Under stirring, MoS_2 powder (50 mg) was added into the mixture containing 10 mL ethanol and 10 mL DDW. The mixture solution was treated by ultrasonication for 8 h, by using a sonicator (180 W, 40 kHz). Afterward, the product solution was treated by centrifugation at 5000 rpm for 10 min. The centrifugation process was repeated for three times to remove aggregates. The prepared MoS_2 nanosheets were suspended in DDW. The supernatant with 2 mg mL^{-1} of MoS_2 nanosheets was collected for subsequent experiments.

AuNPs-decorated PAMAM dendrimer (AuNPs-PAMAM) was prepared by *in-situ* reduction of $HAuCl_4$ with $NaBH_4$ on dendrimer-based template (Qiu et al., 2016; Sutriyo et al., 2015; Çevik et al., 2016; Kong et al., 2017). $HAuCl_4$ aqueous solution (10 mL, 25 mM) was added into PAMAM dendrimer solution (15 mL, 1.0 wt%) under stirring. The mixture solution was stirred vigorously for 1 h at room temperature, which made $AuCl_4^-$ ions attach to –NH_2 groups on dendrimer. Then, 0.5 M of $NaBH_4$ aqueous solution was drop-by-drop added in the mixture solution under stirring. With the reaction proceeding, Au^{3+} ions were reduced to Au^0, together with the change of reaction solution color from pale yellow to red-brown color. Afterward, the product suspension was treated by evaporation to remove most of solvents, followed by centrifugation to obtain aggregates. The aggregates were washed with ethanol and DDW repeatedly, followed by drying at 60 °C to form AuNPs-PAMAM solid products. The products were dispersed in DDW for further use.

To prepare AuNPs-PAMAM/MoS_2 (Kong et al., 2017), 10 mg AuNPs-PAMAM was dispersed in 5 mL DDW to generate a homogeneous aqueous suspension under stirring. The suspension was drop-by-drop added in aqueous suspension of MoS_2 nanosheets (10 mL, 2 mg mL^{-1}). The mixture solution was sonicated for 30 min, followed by continuous stirring for 12 h. The product solution was purified by centrifugation at 5000 rpm for 10 min. The precipitates were rinsed with DDW repeatedly, followed by freeze-drying to achieve the dried composites of AuNPs-PAMAM/MoS_2. The composites were stored at 4 °C or dispersed in methanol for following studies.

2.4. Preparation of aptamer-AuNPs-PAMAM/MoS_2/GCE sensing platform

A commercial GCE was polished to a mirror-like surface with 0.3 and 0.05 μm wet slurries of α-Al_2O_3. The polished GCE was ultrasonically treated in anhydrous alcohol and DDW for 30 s in sequence, followed by rinsing with DDW and drying under N_2 blowing. Then, 5 μL of Nafion was dropped on GCE surface, followed by drop-casting AuNPs-PAMAM/MoS_2 composites dispersed in methanol (5 μL, 1 mg mL^{-1}). The modified GCE was rinsed with deoxygenated PBS (1 mM, pH 7.4), and naturally dried at room temperature. HS-terminated hairpin-DNA aptamer of IFN-γ was diluted in 10 mM Tris-HCl and incubated at 90 °C for 5 min to produce a hairpin secondary structure. The aliquot of aptamer (20 μL, 12 μM) was drop-casted on AuNPs-PAMAM/MoS_2/GCE surface, maintaining 6 h incubation at 37 °C. The modified GCE was rinsed with PBS and dried under N_2 flow. BSA was treated with a small amount of acetic acid and then dispersed in DDW to prepare BSA solution. Aptamer-AuNPs-PAMAM/MoS_2/GCE surface was treated by drop-casting 20 μL BSA solution (2%), followed by incubation for 1 h at 37 °C. BSA was used as a cross-linker or stabilizer to immobilize interface materials and block active sites on GCE.

2.5. Electrochemical measurements and label-free aptasensor fabrication

CV and EIS curves of the bare GCE and GCE after surface modifications with AuNPs, MoS_2, AuNPs-PAMAM, AuNPs-PAMAM/MoS_2, aptamer-AuNPs-PAMAM/MoS_2, and aptamer-AuNPs- PAMAM/MoS_2/BSA were respectively measured by CHI-660E electrochemical workstation at a scan rate of 50 mV s^{-1}. The bare and modified electrodes were immersed in PBS (1 mM, pH 7.4) containing 1 mM $[Fe(CN)_6]^{3-/4-}$ as an electrochemical redox probe. Additionally, aptamer-AuNPs-PAMAM/MoS_2/GCE fixed with BSA was immersed in PBS. MB was added and reached 1 mM in the mixture solution. SWV curves were measured under various conditions, including different pH values, aptamer contents, incubation times and temperatures. IFN-γ was added into the mixture solution and its final content ($\boldsymbol{C}_{\text{IFN-}\gamma}$) varied from 0 to 1000 pg mL^{-1}. Under optimal experiment conditions, SWV curves of aptamer-AuNPs-PAMAM/MoS_2/MB/GCE were measured with each increment of $\boldsymbol{C}_{\text{IFN-}\gamma}$. By plotting a linear relationship between relative peak current intensity ($I–I_0$, where I_0 and I were peak current intensities before and after the addition of targets) of MB and logarithm of $\boldsymbol{C}_{\text{IFN-}\gamma}$ ($\lg\boldsymbol{C}_{\text{IFN-}\gamma}$) in a specific range of $\boldsymbol{C}_{\text{IFN-}\gamma}$, a novel and label-free electrochemical aptasensor of IFN-γ was fabricated.

2.6. Analytical performance and detection applications in real samples

Aptamer-AuNPs-PAMAM/MoS_2/MB/GCE served as a label-free aptasensor and was applied to electrochemical sensing of IFN-γ and potential interferents. Upon the presence of AA, L-cys, UA, glucose,

myoglobin, BSA, Ig G, IL-22 (the each interferent, 4 ng mL^{-1}), IFN-γ (40 pg mL^{-1}) and IFN-γ *plus* the mixture containing eight interferents (32 ng mL^{-1}), SWV curves were measured and the relative redox peak current intensities ($I–I_0$) of MB were calculated. $I–I_0$ changes produced from different components were compared to evaluate selectivity and sensitivity of the aptasensor. IFN-γ detection in real (fresh human serum, urine fluid) samples was performed. The samples were 10-fold diluted with PBS (1 mM, pH 7.4) to prepare sample solutions. SWV curves were measured in the absence and presence of IFN-γ at different coexisting concentrations. $C_{IFN-\gamma}$ in sample solutions was calculated by a plotting linear relationship of $I–I_0$ of MB *versus* $\lg C_{IFN-\gamma}$. Electrochemical curves were measured repeatedly. Each result was expressed as the average of six repeated experiments.

3. Results and discussion

3.1. Preparation and characterization of electroactive materials

UV–vis absorption spectra were characterized in Fig. 1A. In the spectra of PAMAM, a typical absorption band was found at 285 nm. Before reduction, $AuCl_4^-$ ions have a sharp peak at 300 nm. After reduction with $NaHB_4$, the spectrum changes remarkably. The band of $AuCl_4^-$ ions at 300 nm vanished and new absorption bands appeared at 240 and 550 nm. The former originates from a blue-shifted characteristic band of PAMAM from AuNPs-caused changes. The latter originates from the characteristic absorption band of AuNPs (Qiu et al., 2016; Sutriyo et al., 2015). FT-IR spectra were characterized in Fig. 1B. PAMAM dendrimers have characteristic peaks at 1645 and 1574 cm^{-1}, which are assigned to the two bands of amides (I) and (II). A vibration peak at 1394 cm^{-1} is attributed to the terminated carboxylate groups of PAMAM dendrimers. A new and strong vibration peak at 1635 cm^{-1} is assigned to the interactions of AuNPs and PAMAM. These results reveal the preparation of AuNPs-PAMAM composites.

Morphologies and microstructures were characterized by TEM images. In Fig. 2A, MoS_2 shows a typical sheet-like and wrinkled structure (Kong et al., 2017). TEM images of AuNPs-PAMAM composites (Fig. 2B) display the partially aggregated nanoparticles (NPs) with a major diameter distribution of 30–50 nm and an average diameter of ~40 nm. The aggregation originates from AuNPs *in-situ* formed in the matrix of PAMAM dendrimers. Several AuNPs may be prepared in one PAMAM molecule. After the addition of AuNPs-PAMAM on MoS_2 nanosheets, the resulting complex (Fig. 2C) presents many observable NPs that were widely distributed on the surface of sheet-like and wrinkled nanosheets (Jin et al., 2018b). In terms of preparation principle and TEM images (Fig. 2A and B), the aggregated NPs are assigned to AuNPs stabilized in PAMAM, while the sheet-like and wrinkled nanomaterials should be MoS_2 nanosheets. The characterization results confirmed the successful preparation of MoS_2 nanosheets, AuNPs-PAMAM composites and AuNPs-PAMAM/MoS_2 complex.

Under different experiment conditions, the preparation process of products was investigated by TEM images. The prepared products of MoS_2 nanosheets exhibited the sheet-like and aggregated morphology, when the time of ultrasonication liquid-phase exfoliation reached up to 2 h (Fig. S1A in Electronic Supplementary Material (ESM)). With the extending of ultrasonication time to 4 h, the morphology of products with sheet-like structure and little aggregation was observable (Fig. S1B in ESM). After 8 h of ultrasonication exfoliation, the products displayed the typical sheet-like and wrinkled structure (Fig. 2A). The results implied that an extending ultrasonication time can facilitate efficient exfoliation of MoS_2 powder into nanosheets with characteristic morphologies and microstructures. Under magnification multiple, the prepared composites of AuNPs-PAMAM showed several aggregated NPs. which was due to the encapsulation of AuNPs into the matrix of PAMAM dendrimers (Fig. S1C in ESM). With the increase of AuNPs-PAMAM dosage, more NPs were added onto MoS_2 nanosheets to prepare AuNPs-PAMAM/MoS_2 complex, which meanwhile led to the excessive NPs staying far away from nanosheets (Fig. S1D in ESM). Under appropriate dosages of precursors and preparation conditions, superior morphologies and microstructures of the prepared products were achieved in this work (Fig. 2).

3.2. Electrochemical characterization of GCE modified with electroactive materials

The modification process on GCE surface was characterized by electrochemical measurements. Bare GCE and modified GCE were immersed in PBS containing $[Fe(CN)_6]^{3-/4-}$ as a redox probe. Under different conditions, CV and EIS curves of modified electrodes were measured. In Fig. 3A, AuNPs-PAMAM/MoS_2/GCE (curve c) has an improved cathodic peak current from characteristic electrochemical redox of $[Fe(CN)_6]^{3-/4-}$, when compared to AuNPs-PAMAM (curve d) and MoS_2 (curve g). Synergistic enhanced effects of electroactive AuNPs in PAMAM and MoS_2 promote the electrical conductivity of AuNPs-PAMAM/MoS_2 complex. The complex elevates charge transfer rates and enlarges electrode effective areas on GCE surface, which thus facilitate sensitive signal responses during electrochemical sensing (Jin et al., 2018b; Gao et al., 2019). BSA was employed to immobilize the complex on GCE surface. IFN-γ aptamer (curve f) was coupled with AuNPs. The cathodic peak current of aptamer-AuNPs-PAMAM/MoS_2/BSA/GCE is lower than that of the AuNPs-PAMAM/MoS_2/GCE. The fixing and coupling action may block the electron transfer of $[Fe(CN)_6]^{3-/4-}$ probe.

In Fig. 3B, the interface properties of different modified electrodes

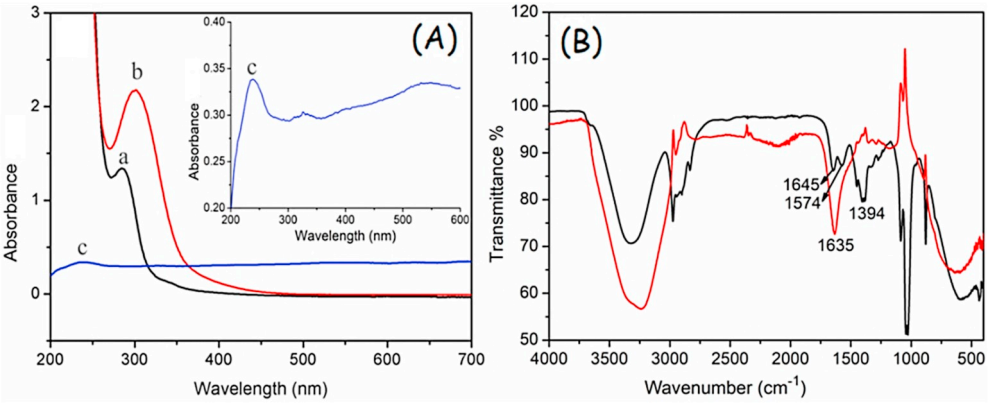

Fig. 1. (A) UV–vis absorption spectra of (a) PAMAM, (b) $HAuCl_4$ and (c) AuNPs-PAMAM. Insert is the amplified figure of curve (c). (B) FT-IR spectra of PAMAM (black curve) and AuNPs-PAMAM (red curve). (For interpretation of the references to color in this figure legend, the reader is referred to the Web version of this article.)

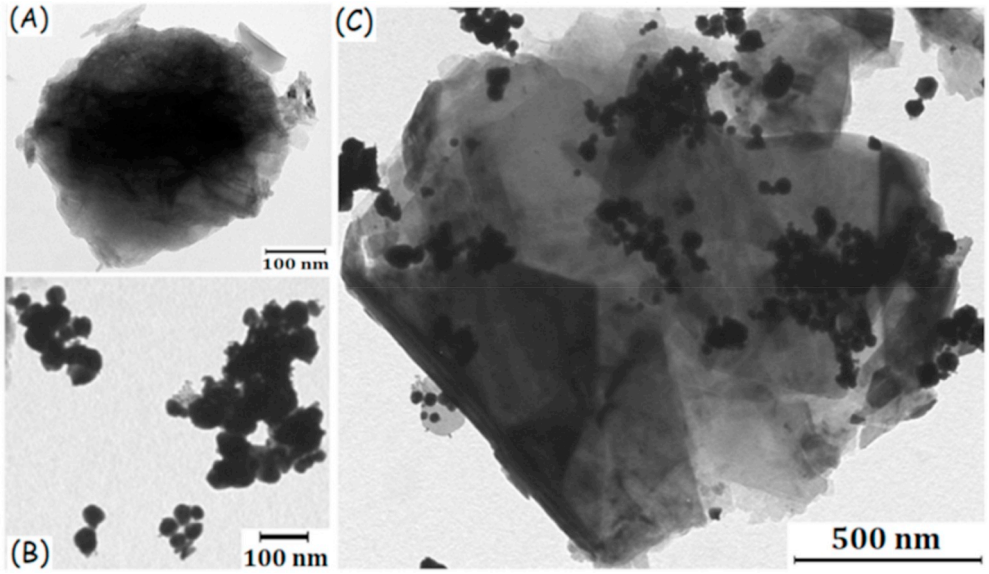

Fig. 2. TEM images of MoS_2 (A), PAMAM-AuNPs (B) and AuNPs-PAMAM/MoS_2 (C).

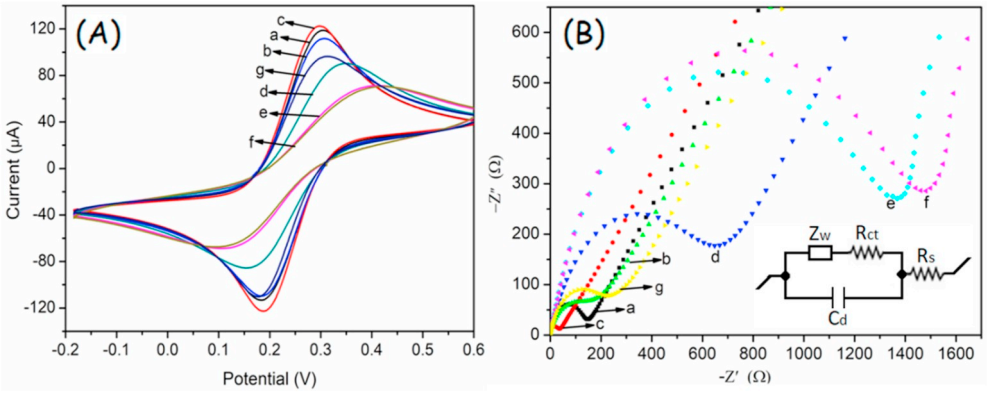

Fig. 3. (A) CV and (B) EIS curves measured from different modified electrodes of bare GCE (a), GCE modified with AuNPs (b), AuNPs-PAMAM/MoS_2 (c), AuNPs-PAMAM (d), aptamer-AuNPs-PAMAM/MoS_2 (e), aptamer- AuNPs-PAMAM/MoS_2/BSA (f) and MoS_2 (g). Randles equivalence circuit model inserted in (B) was used to fit the data.

were characterized by EIS curves. The charge transfer resistance (R_{ct}) depends on electron transfer kinetics of redox probes at electrode interfaces. R_{ct} is calculated through semicircle diameters of the Nyquist diagram. After modification on GCE surface with different electroactive materials, large semicircular domains appear and indicate the resistance of charge transfer. R_{ct} of AuNPs-PAMAM/MoS_2/GCE (curve c) is lower than that of AuNPs-PAMAM (curve d) and MoS_2 (curve g). R_{ct} of the aptamer-AuNPs- PAMAM/MoS_2/BSA/GCE is higher than that of AuNPs-PAMAM/MoS_2/GCE. These typical EIS results are well consistent with CV results. As reciprocal parameters of R_{ct} and redox peak current, their change trends are opposite reasonably (Gao et al., 2018). The CV and EIS results adequately verify the preparation of aptamer--AuNPs-PAMAM/MoS_2/GCE sensing platform.

3.3. Optimal conditions for electrochemical measurements of modified electrodes

As for AuNPs-PAMAM/MoS_2/MB/GCE sensing platform, various experiment conditions were optimized by measuring SWV curves (Gao et al., 2018; Jin et al., 2018a). When the modified GCE was immersed into deoxygenated PBS (1 mM) at different pH values, SWV curves were measured (Fig. 4A). When pH varies from 6 to 8, the peak current of MB reaches the maximum at pH 7.4. At the optimal pH, 20 μL aptamer was drop-casted onto AuNPs-PAMAM/MoS_2/GCE surface to form aptamer-AuNPs-PAMAM/MoS_2/MB/GCE. With each increment of aptamer concentration to 12 μM, the highest peak current of MB was obtained (Fig. 4B). During SWV measurements, the incubation time and temperature were studied. At the optimal pH (7.4) and aptamer concentration (12 μM), the peak current intensities of MB can reach the maximum when the modified GCE was incubated for 6 min at 37 °C (Fig. 4C and D).

The concentration of MB (C_{MB}) used to construct the new sensing platform was optimized by measuring SWV curves. MB as a redox probe was absorbed on the aptamer. The peak current of MB gradually increased with each increment of C_{MB} and reached the equilibrium value at 1 mM (Fig. 4E). Afterward, a continuous increase of C_{MB} (2 and 5 mM) only caused negligible changes of the peak current intensities, indicating the adsorption equilibrium of MB. Excessive MB hardly influenced on the redox process of MB on GCE surface and cannot produce dramatically changed electrochemical signal. Thus, 1 mM was considered as the optimal C_{MB}. In this case, the prepared aptamer-AuNPs-PAMAM/MoS_2/MB/GCE sensing platform was incubated in PBS (1 mM, pH 7.4) as electrolyte solution for different times. With the extending of incubation time from 1 to 6 min, the peak current of MB increased regularly (Fig. 4F). A further incubation time more than 6 min did not result in a remarkable change of the peak current. These results revealed that the

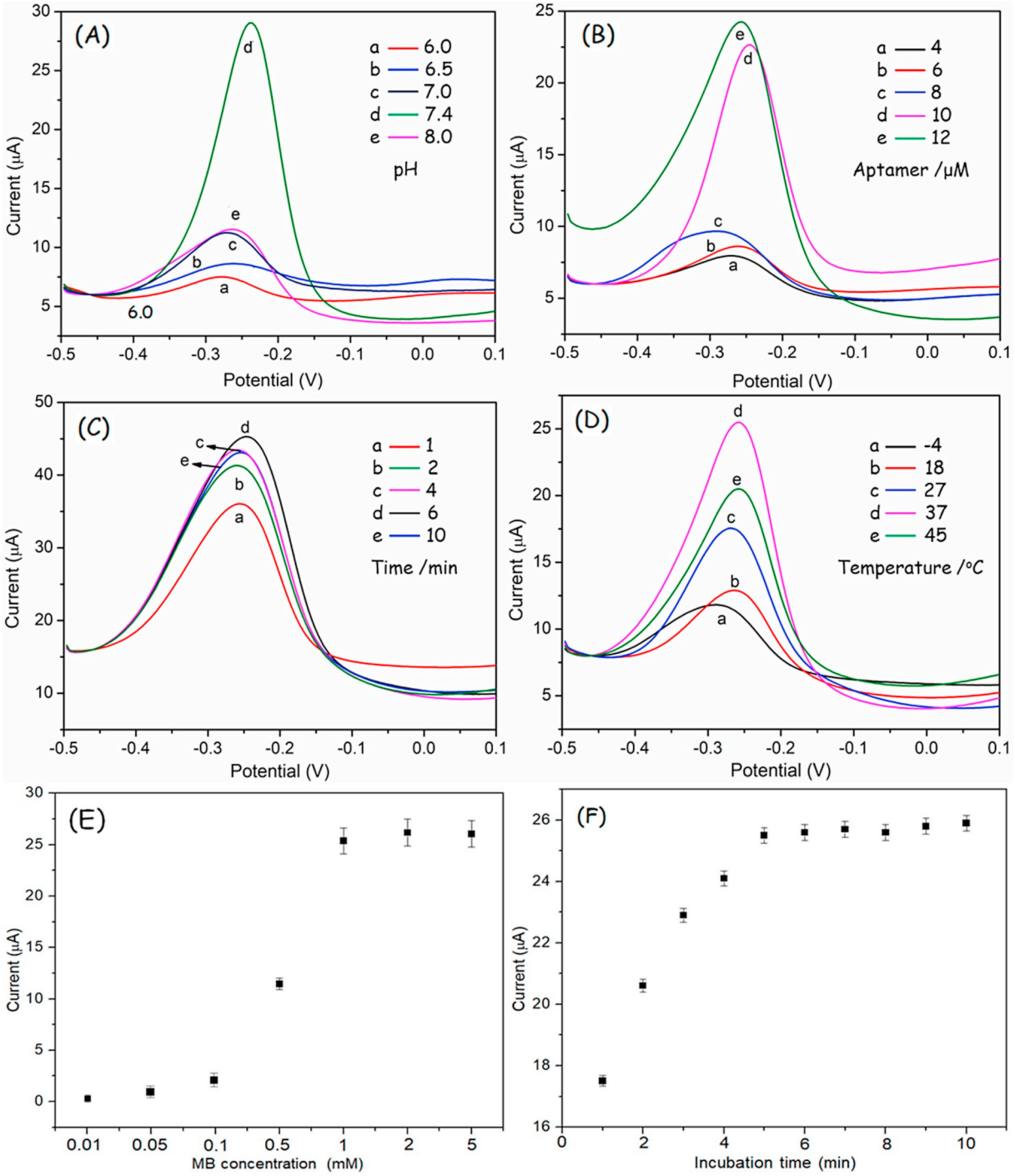

Fig. 4. SWV curves of AuNPs-PAMAM/MoS_2/MB/GCE prepared under different conditions: immersed in 1 mM PBS at different pH values (A), drop-casting 20 μL aptamer of different concentrations (B), incubated for different times (C) and at different temperatures (D) before electrochemical measurements. The peak current intensities of aptamer-AuNPs-PAMAM/MoS_2/MB/GCE in the presence of MB at different coexisting concentrations (E) with 6 min of incubation and at different incubation times (F) containing 1 mM of MB.

optimal incubation time was 6 min. Under optimal conditions, this aptamer-AuNPs-PAMAM/MoS_2/MB/GCE as a new sensing platform was developed as novel single-amplified and label-free aptasensor for electrochemical sensing of IFN-γ.

3.4. Fabrication method of label-free electrochemical aptasensor of IFN-γ

The aptamer-AuNPs-PAMAM/MoS_2/MB/GCE was immersed in deoxygenated PBS electrolyte solution with addition of IFN-γ. SWV curves were measured under optimal conditions (Fig. 5A). Redox peak current intensities of MB increased gradually with increase of $C_{IFN\text{-}\gamma}$. In the presence of IFN-γ, specific coupling of IFN-γ with its aptamer triggered the hairpin conformation transform of IFN-γ aptamer to a linear conformation. The transform action is competitively stronger than the action of base complementary pairing in hairpin aptamer. A linear aptamer has superior adsorption capability over a hairpin one. In the presence of IFN-γ, there is a specific coupling of IFN-γ with its aptamer. Meanwhile, the increasing MB was absorbed on linear aptamer, which

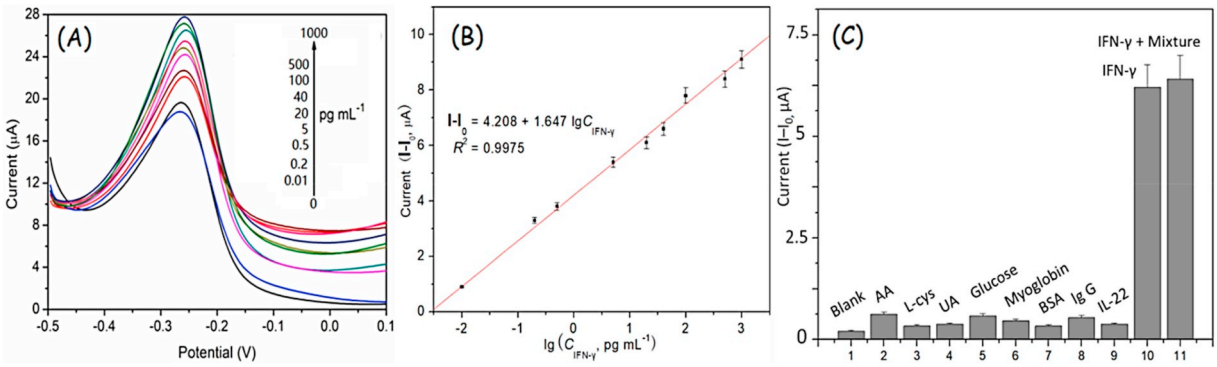

Fig. 5. (A) SWV curves of AuNPs-PAMAM/MoS_2/MB/GCE in the presence of IFN-γ at different concentrations. (B) A well plotting linear relationship between relative peak current intensity (I–I_0) of MB and lg$C_{IFN-γ}$ in the range from 0 to 1000 pg mL^{-1} of IFN-γ. (C) Relative redox peak current intensities of MB measured without (blank) and with the presence of each interferent (4 ng mL^{-1}), IFN-γ (40 pg mL^{-1}) and IFN-γ *plus* the mixture containing eight interferents (32 ng mL^{-1}).

thus enhanced electrochemical redox signal of MB. There is a well plotting linear regression curve ($R^2 = 0.9975$) between relative peak current intensities (I–I_0) of MB and lg$C_{IFN-γ}$ in a specific $C_{IFN-γ}$ range from 0 to 1000 pg mL^{-1} (Fig. 5B). The limit of detection (LOD) was approximately 2 fg mL^{-1}, calculated based on signal-to-noise ratio ($S/N = 3$). In terms of the linear regression curve, an amplified label-free electrochemical aptasensor of IFN-γ was fabricated by using the sensing platform of aptamer- AuNPs-PAMAM/MoS_2/MB/GCE. As briefly summarized in Table S1 (ESM), the detection range of $C_{IFN-γ}$ is comparable to that from the previously reported electrochemical methods (Abnous et al., 2017; Ding et al., 2017; Zhang et al., 2015, 2016; Zhu et al., 2016; Liu et al., 2010, 2015a; Farid et al., 2015; Miao et al., 2017). By contrast, this developed aptasensor of IFN-γ had a much low LOD, indicating relatively high detection sensitivity. In this work, the optimal incubation time (6 min) before the sensing measurements of IFN-γ is much shorter than that of previous methods for IFN-γ determination.

3.5. Selectivity, sensitivity and stability of this aptasensor for IFN-γ detection

To investigate the electrochemical signal responses of this aptasensor, SWV curves of aptamer- AuNPs-PAMAM/MoS_2/MB/GCE were measured in the presence of IFN-γ and interferents (AA, L-cys, UA, glucose, myoglobin, BSA, Ig G, IL-22). Relative peak current intensities (I–I_0) of MB were compared to evaluate the selectivity and sensitivity of this aptasensor for IFN-γ detection. As summarized in Fig. 5C, the addition of each interferent (4 ng mL^{-1}) did not induce an obvious impact on I–I_0 values (0.5–0.8), when compared with the blank without the addition of IFN-γ or interferents (0.3). By contrast, the addition of IFN-γ at 40 pg mL^{-1} led to a remarkable change of I–I_0 (~6.4). Upon simultaneous addition of IFN-γ and eight interferents (32 ng mL^{-1}), the caused change of I–I_0 is ~6.8 that is close to that from the only addition of IFN-γ without interferents. The interferents even coexisting at 100-fold or 800-fold higher concentrations than IFN-γ only made negligible influences on I–I_0. The results verified high performance of this aptasensor for sensitive and selective determination of IFN-γ, over potential interferents. In addition, the stability of this aptasensor was evaluated. The aptamer-AuNPs-PAMAM/MoS_2/MB/GCE was placed in the dark at 4 °C and was covered with a breaker. After incubation for two weeks, a clean electrode surface was maintained always. SWV curves of this modified GCE were measured to achieve the redox peak current intensities of MB. The relative standard deviation (RSD, $n = 6$) was calculated to be ~2.1%. The low RSD suggests high stability and repeatability of this sensing platform. The results testify high feasibility of the aptamer-AuNPs-PAMAM/MoS_2/MB/GCE for efficient determination of IFN-γ.

3.6. Detection performance of IFN-γ in real samples based on this aptasensor

To further study the practicability of this sensing platform for IFN-γ detection, the contents of IFN-γ in real samples (human serum and urine fluids) without and with the addition of IFN-γ were determined by using the plotting linear regression curve between relative peak current intensities (I–I_0) of MB and lg$C_{IFN-γ}$ (in Fig. 5B). As summarized inTable S2 (ESM), the detected results of $C_{IFN-γ}$ were in good agreement with the spiked ones, accompanying with high detection recoveries of 95.2–105.0% and low RSD of 1.59–4.78% ($n = 6$). Furthermore, the real samples without and with the addition of IFN-γ were detected by enzyme-linked immunosorbent assay (ELISA) method. Through ELISA test, the obtained results of $C_{IFN-γ}$ were close to the spiked results. Meanwhile, the results of $C_{IFN-γ}$ detected by this aptasensor were comparable with those obtained by ELISA test as a standard reference method. The results indicated this aptasensor could have a potential application in clinical diagnostics of IFN-γ. High agreement between the detected and spiked results of $C_{IFN-γ}$ effectively testified that the signal-amplified and label-free electrochemical aptasensor based on aptamer-AuNPs-PAMAM/MoS_2/MB/GCE sensing platform had excellent performance for IFN-γ determination in real biological samples and had high reliability and practicability.

4. Conclusions

In summary, a novel and signal-amplified label-free electrochemical aptasensor was developed for sensitive detection of IFN-γ, based on aptamer-AuNPs-PAMAM/MoS_2/MB/GCE as a sensing platform. AuNPs were electrodeposited in the matrix of PAMAM dendrimers. After drop-by-drop addition of AuNPs-PAMAM on MoS_2 nanosheets, AuNPs-PAMAM/MoS_2 was dropped-casting on Nafion-modified GCE interface. HS-terminated hairpin-DNA aptamer of IFN-γ was conjugated with AuNPs *via* Au–S coupling to prepare aptamer-AuNPs-PAMAM/MoS_2/GCE, by using BSA as a cross-linker or stabilizer. MB was absorbed on IFN-γ aptamer and showed weak electrochemical signal of MB. In the presence of IFN-γ, hairpin conformation of single-strand DNA aptamer was transferred into linear one. The transform was due to specific coupling of IFN-γ with its aptamer, which was stronger than that of base complementary pairing in hairpin aptamers. Linear aptamers have superior adsorption over hairpin ones. The increasing MB was absorbed on linear aptamers, with improved electrochemical signal of MB. With each increment of $C_{IFN-γ}$, MB electrochemical signal increased regularly. There is a well plotting linear relationship between relative peak current intensities of MB and lg$C_{IFN-γ}$ in the $C_{IFN-γ}$ range of 0.01–1000 pg mL^{-1}, with a low LOD of 2 fg mL^{-1}. This aptasensor had selective and sensitive responses on IFN-γ, over potential interferents. In real biological fluids, this aptasensor had superior performance for IFN-γ detection, indicating

its high reliability and practicability.

Declaration of competing interest

The authors declare that they have no known competing financial interests or personal relationships that could have appeared to influence the work reported in this paper.

Acknowledgements

This work was financially supported by the Natural Science Foundation of Shandong Province (ZR2019MB026) and the Source Innovation Plan Application Basic Research Project of Qingdao (17-1-1-72-jch, 18-2-2-26-jch).

Appendix A. Supplementary data

Supplementary data to this article can be found online at https://doi.org/10.1016/j.bios.2019.111732.

References

Abnous, K., Danesh, N.M., Ramezani, M., Alibolandi, M., Hassanabad, K.Y., Emrani, A.S., Bahreyni, A., Taghdisi, S.M., 2017. Microchim. Acta 184, 4151–4157.
Akter, F., Mie, M., Grimm, S., Nygren, P.Å., Kobatake, E., 2012. Anal. Chem. 84, 5040–5046.
Biron, C.A., Nguyen, K.B., Pien, G.C., Cousens, L.P., Salazar-Mather, T.P., 1999. Annu. Rev. Immunol. 17, 189−–220.
Boehm, U., Klamp, T., Groot, M., Howard, J.C., 1997. Annu. Rev. Immunol. 15, 749–795.
Çevik, E., Bahar, Ö., Şenel, M., Abasıyanık, M.F., 2016. Biosens. Bioelectron. 86, 1074–1079.
Cohen, L., Walt, D.R., 2018. Bioconjug. Chem. 29, 3452–3458.
Ding, S., Mosher, C., Lee, X.Y., Das, S.R., Cargill, A.A., Tang, X., Chen, B., McLamore, E. S., Gomes, C., Hostetter, J.M., Claussen, J.C., 2017. ACS Sens. 2, 210–217.
Dowlati, Y., Herrmann, N., Swardfager, W., Liu, H., Sham, L., Reim, E.K., Lanctôt, K.L., 2010. Biol. Psychiatry 67, 446–457.
Farid, S., Meshik, X., Choi, M., Mukherjee, S., Lan, Y., Parikh, D., Poduri, S., Baterdene, U., Huang, C.E., Wang, Y.Y., Burke, P., Dutta, M., Stroscio, M.A., 2015. Biosens. Bioelectron. 71, 294–299.
Gao, X., Gui, R., Guo, H., Wang, Z., Liu, Q., 2019. Sens. Actuators, B 285, 201–208.
Gao, X., Gui, R., Xu, K.Q., Guo, H., Jin, H., Wang, Z., 2018. New J. Chem. 42, 14796–14804.
Golichenari, B., Nosrati, R., Farokhi-Fard, A., Abnous, K., Vaziri, F., Behravan, J., 2018. Biosens. Bioelectron. 117, 319–331.
Guo, H., Gui, R., Jin, H., Wang, Z., 2017. New J. Chem. 41, 9977–9983.
Guo, H., Jin, H., Gui, R., Wang, Z., Xia, J., Zhang, F., 2017. Sens. Actuators, B 253, 50–57.
Jager, W.D., Velthuis, H.T., Prakken, B.J., Kuis, W., Rijkers, G.T., 2003. Clin. Diagn. Lab. Immunol. 10, 133–139.
Jin, H., Gui, R., Yu, J., Lv, W., Wang, Z., 2017. Biosens. Bioelectron. 91, 523–537.
Jin, H., Guo, H., Gao, X., Gui, R., 2018. Sens. Actuators, B 277, 14–21.
Jin, H., Zhao, C., Gui, R., Gao, X., Wang, Z., 2018. Anal. Chim. Acta 1025, 154–162.
Kong, L., Xing, L., Zhou, B., Du, L., Shi, X., 2017. ACS Appl. Mater. Interfaces 9, 15995–16005.
Li, X., Du, X., 2017. Sens. Actuators, B 239, 536–543.
Liu, C., Xiang, G., Jiang, D., Liu, L., Liu, F., Luo, F., Pu, X., 2015. Analyst 140, 7784–7791.
Liu, Y., Liu, Y., Matharu, Z., Rahimian, A., Revzin, A., 2015. Biosens. Bioelectron. 64, 43–50.
Liu, Y., Tuleouva, N., Ramanculov, E., Revzin, A., 2010. Anal. Chem. 82, 8131–8136.
Miao, X., Ko, C.N., Vellaisamy, K., Li, Z., Yang, G., Leung, C.H., Ma, D.L., 2017. Sci. Rep. 7, 42740.
Omae, T., Saito, Y., Tsuchie, H., Ohno, K., Maegaki, Y., Sakuma, H., 2018. Brain Dev. 40, 361–365.
Qiu, Z., Tang, D., Shu, J., Chen, G., Tang, D., 2016. Biosens. Bioelectron. 75, 108–115.
Schroder, K., Hertzog, P.J., Ravasi, T., Hume, D.A., 2004. J. Leukoc. Biol. 75, 163–189.
Shamsipur, M., Farzin, L., Tabrizi, M.A., Molaabasi, F., 2015. Biosens. Bioelectron. 74, 369–375.
Sutriyo, Mutalib, A., Ristaniah, Anwar, E., Radji, M., Pujiyanto, A., Purnamasari, P., Joshita, D., Adang, H.G., 2015. Macromol. Symp. 353, 96–101.
Wang, Z., Yu, J., Gui, R., Jin, H., Xia, Y., 2016. Biosens. Bioelectron. 79, 136–149.
Wen, D., Liu, Q., Cui, Y., Kong, J., Yang, H., Liu, Q., 2018. Sens. Actuators, B 276, 279–287.
Xia, J., Song, D., Wang, Z., Zhang, F., Yang, M., Gui, R., Xia, L., 2015. Biosens. Bioelectron. 68, 55–61.
Yan, G., Wang, Y., He, X., Wang, K., Liu, J., Du, Y., 2013. Biosens. Bioelectron. 44, 57–63.
Zhang, Y., Yan, Y., Zhang, B., Zhu, W., He, Y., Huang, H., Li, J., Jiang, Z., Tan, S., Cai, X., 2015. J. Solid State Electrochem. 19, 3111–3119.
Zhang, Y., Zhang, B., Ye, X., Yan, Y., Huang, L., Jiang, Z., Tan, S., Cai, X., 2016. Mater. Sci. Eng. C 59, 577–584.
Zhou, K., Zhang, Q., Liu, J., Wang, B., Jiang, S., Shi, Y., Hu, Y., Gui, Z., 2014. RSC Adv. 4, 13205–13214.
Zhou, Q., Lin, Y., Zhang, K., Li, M., Tang, D., 2018. Biosens. Bioelectron. 101, 146–152.
Zhu, M., Tang, Y., Wen, Q., Li, J., Yang, P., 2016. Microchim. Acta 183, 1739–1748.